Impact of Grain Boundaries on the Electronic Properties and Schottky Barrier Height of MoS_2@Au Heterojunctions

Abstract

Viacheslav Sorkin[1,1], Hangbo Zhou[1], Zhi Gen Yu[1], Kah-Wee Ang[2,3,2], Yong-Wei Zhang[1,3]

Supplementary Materials

Electronic structure for free-standing MoS_2 monolayer with zigzag grain boundaries

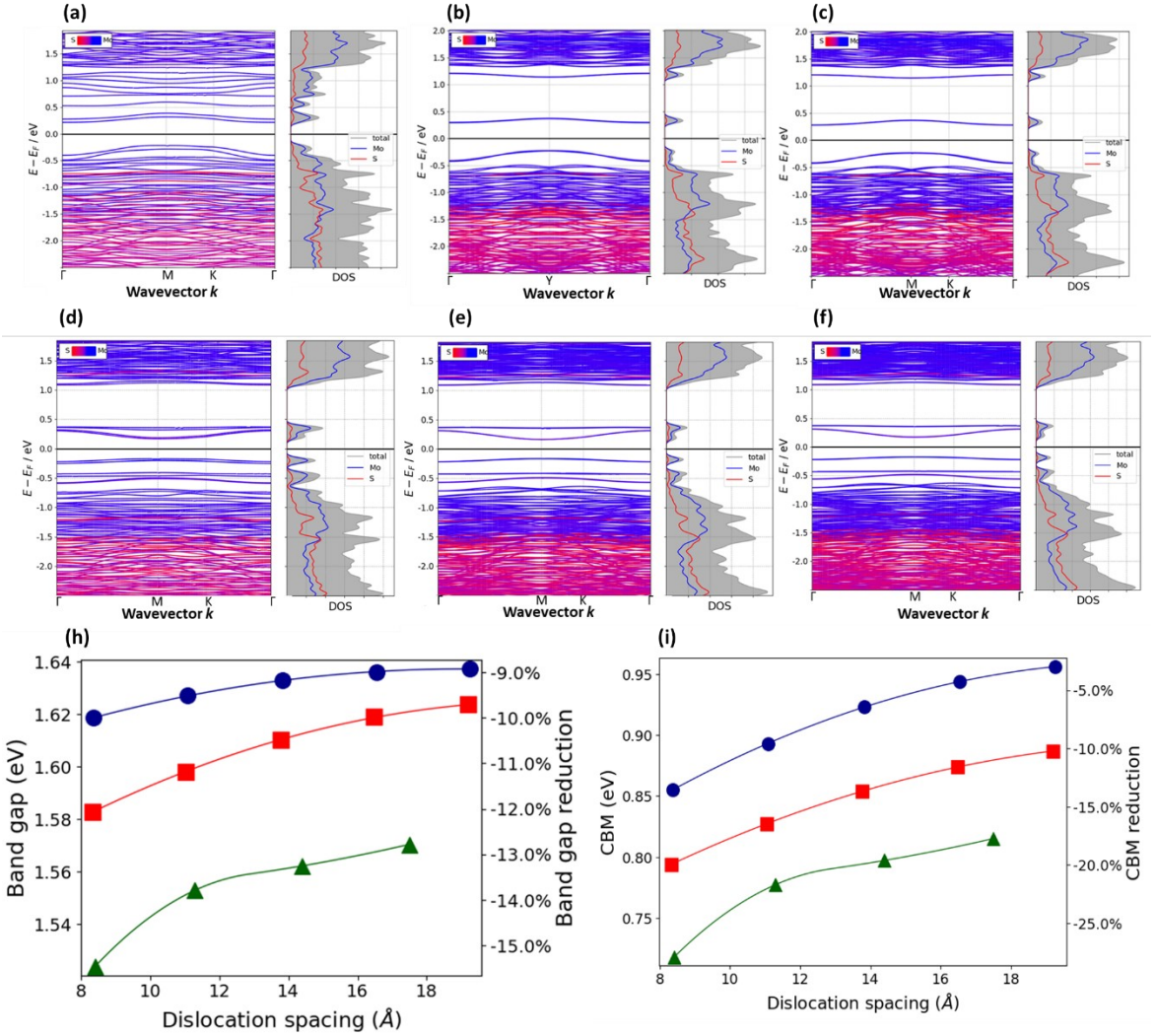

[1] Email: sorkinv@ihpc.a-star.edu.sg
[2] Email: eleakw@nus.edu.sg
[3] Email: zhangyw@ihpc.a-star.edu.sg

Figure S1: (a-c) Electronic band structure (EBS; left panel) and density of states (DOS; right panel) for free-standing MoS_2 layers with ZZ GBs formed by two periodic arrays of equidistant (4|8) edge dislocations. The dislocation spacing is one hexagon. The distance between the GBs is four (a), five (b), and six (c) hexagonal units. (d-f) EBS and DOS for free-standing MoS_2 layers with ZZ GB formed by two periodic arrays of adjacent (5|7) edge dislocation pairs appeared after structural reconstruction of (4|8) dislocations. The dislocation spacing is two hexagons, and the distance between the GBs is four (d), five (e), and six (f) hexagonal units. The partial DOS is calculated as an average over the d-orbitals of Mo atoms (blue) and the p-orbitals of S atoms (red). The total DOS is represented by the grey shaded region. (h) Impact of dislocation spacing on band gap size (h) and CBM (i) of MoS_2 monolayer containing (5|7) AC GBs (blue circles), (4|6)/(6|8) AC GBs (red squares), and (4|8) ZZ GBs (green triangles). The right-hand axis shows the relative percentage decrease of the band gap compared to the pristine MoS_2 monolayer.

Sublayer spacing ratio

To examine the change in the configuration of Au-supported MoS_2 monolayer, we measured the distances between the top S plane and the middle Mo plane, D_t, and between the bottom S sublayer and the middle Mo layer, D_b, using the average Z-coordinates of the atoms in the corresponding planes (Figure S2(a)). We calculated the ratio D_t/D_b, which is equal to the one for free-standing MoS_2. As shown in Figure S2(b), the ratio increases with decreasing dislocation spacing: a larger deviation from unity indicating a stronger interaction.

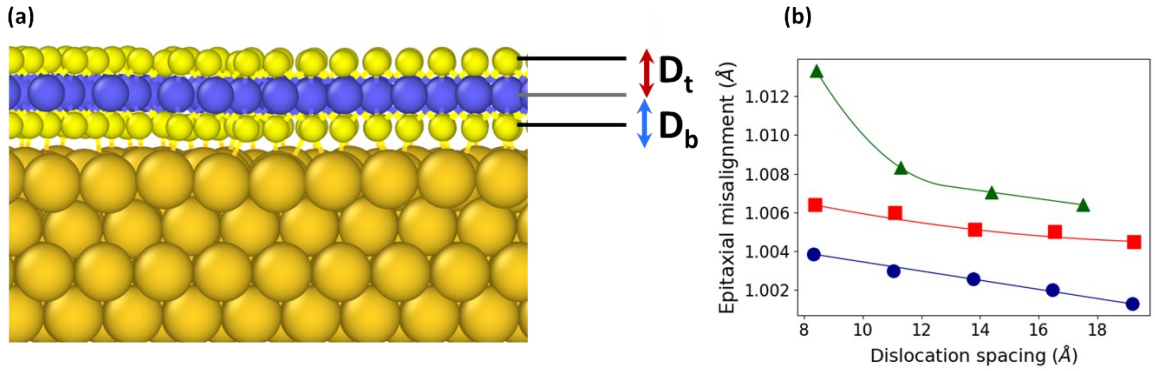

Figure S2: (a) Schematic diagram of a MoS2@Au(111) heterojunction, with the distances between the top S sublayer of MoS_2 and the middle Mo sublayer, D_t, and between the bottom S sublayer and the middle Mo layer, D_b, indicate, (b) D_t/D_b ratio plotted as a function of the dislocation spacing at the MoS2@Au junction for MoS_2 with GBs formed by equidistant (4/8) edge dislocations (green triangles), (5/7) dislocations (blue circles), and (4/6) and (6/8) dislocations (red squares).

Electronic structure for Au-supported MoS_2 monolayer with grain boundaries

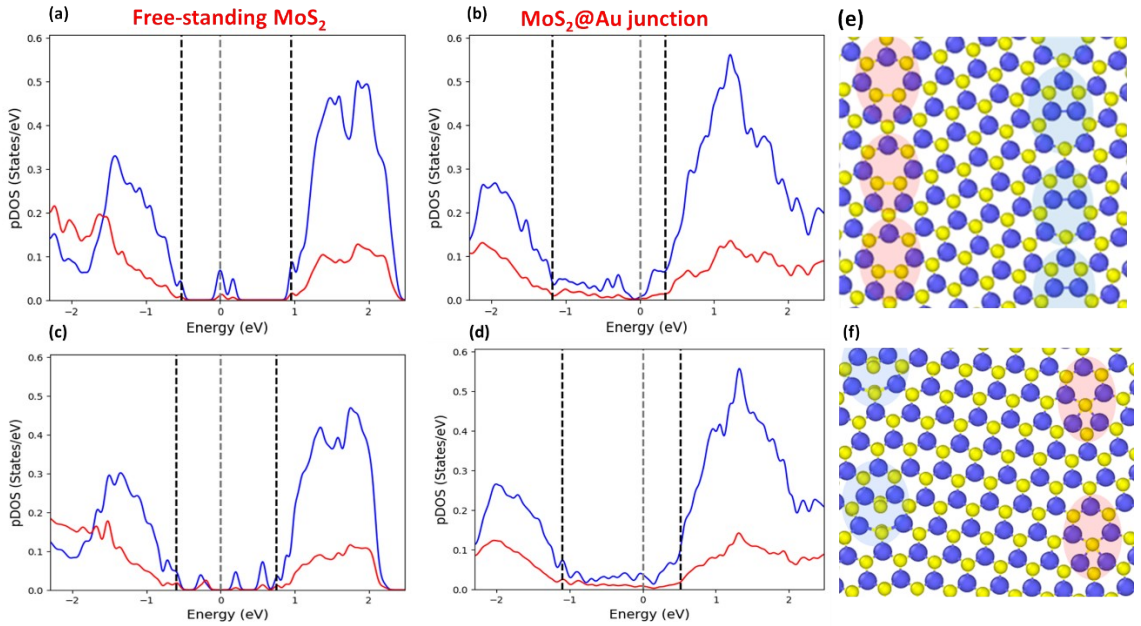

Figure S3: Partial density of states (PDOS) for free-standing and Au(111)-physisorbed MoS_2 monolayers with GBs formed by two parallel periodic arrays of equidistant edge dislocations.(a, b) PDOS for a free-standing and physisorbed MoS_2 monolayer with (5/7) GBs, respectively (c, d) PDOS for a free-standing and physisorbed MoS_2 monolayer with (4/6) and (6|8) GBs, respectively.(e, f) Schematic diagrams of (5/7) and (4/6)(6/8) GBs with opposite orientations, respectively. The shaded areas indicate the dislocations, with red and blue colours denoting dislocations with opposite orientations. The PDOS is calculated as an average over the d-orbitals of Mo atoms (blue) and the p-orbitals of S atoms (red). The valence band maximum (VBM), Fermi level, and conduction band minimum (CBM), obtained using EBS, are shown by dashed lines.

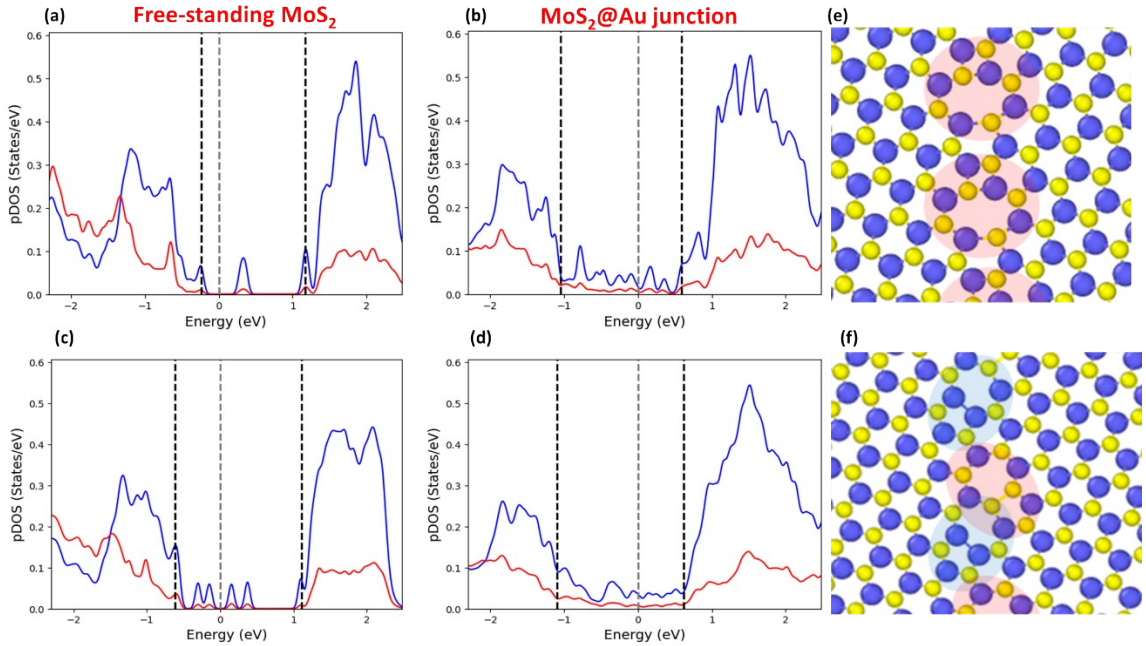

Figure S4: PDOS for free-standing and Au(111)-physisorbed MoS_2 monolayers with GBs formed by two parallel periodic arrays of equidistant (4|8) edge dislocations.(a, b) PDOS for free-standing and Au(111)-physisorbed MoS_2 monolayer with (4/8) GBs separated by a single hexagon along the GB, respectively.(c, d) PDOS for free-standing and Au(111)-physisorbed MoS_2 monolayer with GBs formed by reconstructed (5/7) pairs separated by two hexagons along the GB, respectively.(e, f) Schematic diagrams of (4/8) and 2x(5/7) GBs, respectively. The shaded areas indicate the dislocations. The PDOS is calculated as an average over the d-orbitals of Mo atoms (blue) and the p-orbitals of S atoms (red). The VBM, FL, and CBM, obtained using EBS, are shown by dashed lines.

Charge density minimum at the interface

When a MoS_2 was placed on an Au substrate, charge transferred from the Au to the monolayer due to its higher electronegativity, creating regions of charge accumulation and depletion at the MoS_2@Au interface (Figure S5(a)). A non-zero charge density at the interface is evident in the plane averaged charge density profile along the z-axis (perpendicular to the MoS_2@Au interface, Figure S5(b)). The profile is given by : $\rho(z) = \frac{1}{A}\iint \rho_{MoS_2/Au}(x,y,z)dxdy$, where A is the contact area measured within the [X,Y] plane and $\rho_{MoS_2/Au}(x,y,z)$ is the charge density of the entire sample. The charge density minimum at the interface , $\rho(z_{min})$ and its location of z_{min} are shown in Figure S5(b)).

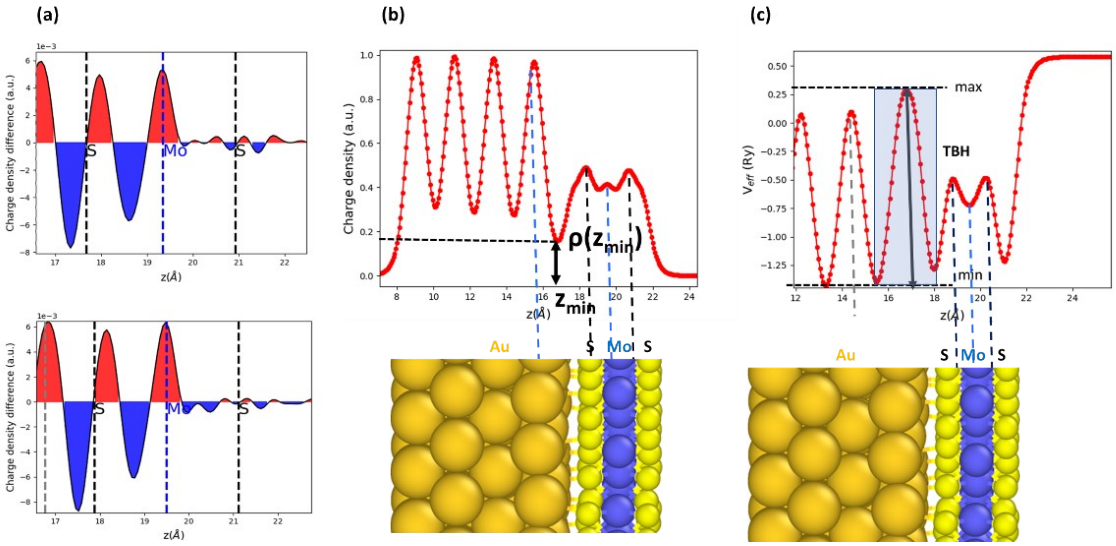

Figure S5: Charge distribution and electrostatic potential of Au(111)-physisorbed MoS_2 monolayers with GBs: (a) Charge density difference for MoS_2 monolayers physisorbed on Au(111) with (5/7) GBs (top panel) and (4/6)(6/8) GBs (bottom panel), revealing regions of charge accumulation (red) and depletion (blue).(b) Top Panel: XY-plane-averaged charge density profile perpendicular to the Au(111)-MoS_2 interface, highlighting the position of the minimum charge density at the interface. Bottom Panel: Schematic diagram of the interface, demonstrating its spatial relationship to the charge density profile. (c) Top Panel: XY-plane-averaged electrostatic potential profile perpendicular to the Au(111)-MoS_2 interface, with the maximum electrostatic potential at the interface and the minimum in the Au substrate indicated. The tunnel barrier height is represented by the difference between these two values. Bottom Panel: Schematic diagram of the interface, illustrating its spatial relationship to the electrostatic potential profile. The physisorbed MoS_2 monolayers in (b) and (c) exhibit GBs formed by two parallel periodic arrays of equidistant (5/7) edge dislocations.

Epitaxial atomic alignment

A free-standing MoS_2 monolayer with grain boundaries was placed on a six-layer Au(111) slab in a configuration that maximizes binding energy per atom, namely : $E_{bind} = \left(E_{MoS_2@Au} - E_{Au} - E_{MoS_2}\right)/N$, where $E_{MoS_2@Au}$ is the total energy of the MoS_2@Au(111) hetero-junction, E_{Au} is the energy of the Au slab, E_{MoS_2} is the energy of MoS_2 monolayer with GBs, and N is the total number of atoms in the sample.

The binding energy of MoS_2 on an Au substrate can be adjusted by changing the relative positions of the bottom plane of S atoms in MoS_2 (closest to the Au substrate) and the top surface plane of Au atoms (Figure S6(a)). This epitaxial alignment is achieved by rotating and shifting the MoS_2 monolayer to maximize the overlap between these atomic planes. To maximize the overlap between the atomic planes, we calculated the total number of van der Waals (vdW) bonds between these atomic planes. Specifically, for each S atom in the bottom plane of MoS_2, we identified a set of Au

atoms at the top surface layer within a selected vdW bond cut-off radius (Figure S6(b)). We then summed the number of bonds for all S atoms. The cut-off radius is the average vdW bond length between the Au atoms of the top surface layers and the S atoms of the bottom plane of pristine defect-free MoS_2 (2.6 Å) taken from[1] .

When constructing MoS_2 samples with grain boundaries, we adjusted the mutual positions of MoS_2 on an Au substrate to maximize the total number of vdW bonds between the bottom plane of S atoms in MoS_2 and the top surface plane of Au atoms. This arrangement was further adjusted during sample relaxation using DFT.

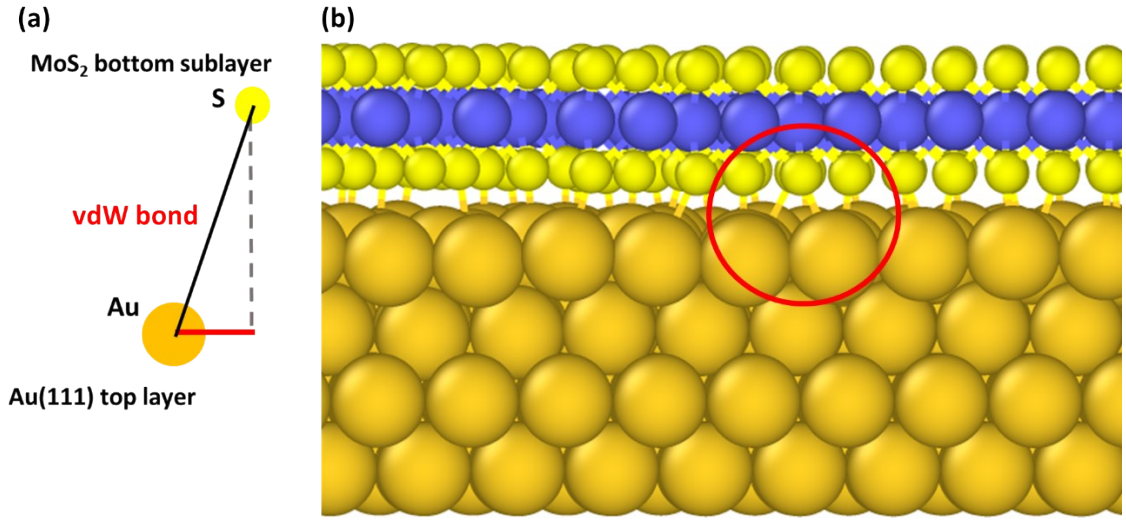

Figure S6: (a) Schematic diagram of a van der Waals (vdW) bond between a S atom in the bottom plane of MoS_2 and an Au atom at the top surface of Au.(b) Schematic diagram of a set of vdW bonds within the selected cut-off radius, indicated by the red circle.

Interface dipole moment

The interface dipole moment, IDM, at the MoS_2@Au interface arises from the combination of charge transfer, rehybridization of atomic orbitals, and surface relaxation of metallic substrate[2–6]. It was calculated by integrating the plane-averaged charge density difference multiplied by the z-coordinate: $IDM = 1/A \iiint z\Delta\rho(x,y,z)dxdydz$, where $\Delta\rho(x,y,z) = \rho_{MoS_2/Au}(x,y,z) - \rho_{Au}(x,y,z) - \rho_{MoS_2}(x,y,z)$ is the difference between the electronic density of the Au substrate, $\rho_{Au}(x,y,z)$ and the MoS_2 monolayer, $\rho_{MoS_2}(x,y,z)$.

Tunnel barrier height

The tunnel barrier at the MoS_2@Au interface affects charge transport by reducing the number of charge carriers and lowering the SBH. We used the contact distance as the barrier width and calculated the barrier height using the Hartree potential, $V(x,y,z)$. The tunnel barrier height (TBH) was obtained as the difference between the maximum of plane averaged electrostatic potential, $V(z) = \frac{1}{A}\iint V(x,y,z)dxdy$, at the MoS_2@Au interface and its minimum in the Au substrate[6,7] (Figure S5(c)).

Electronic structure for free-standing MoS_2 monolayer with arm-chair grain boundaries

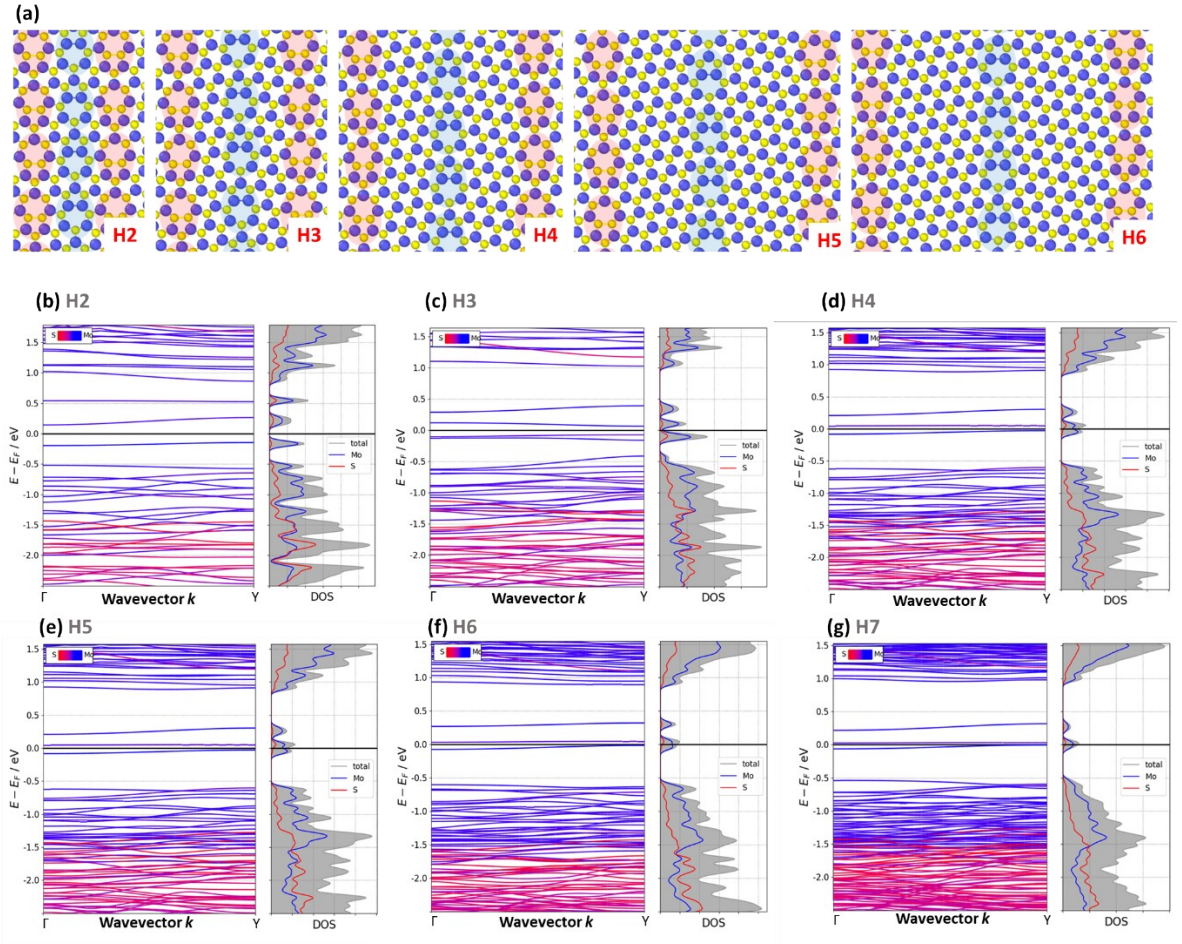

Figure S7: (a) Free-standing MoS_2 layers with GBs formed by two periodic arrays of equidistant (5|7) edge dislocations. The distance between the GBs varies from two hexagons (H2) to six hexagons (H6). The blue regions indicate edge dislocations, characterized by Mo-Mo bonds connecting pentagons and heptagons, while the red regions represent those with S-S bonds. The nearest edge dislocations are separated by a single hexagon along the GB. (b) Electronic band structure (left panel) and DOS (right panel) for the samples described in (a). Partial DOS calculated as an average over d-orbitals of Mo atoms indicated by blue, and over p-orbitals of S atoms specified by red. The total DOS is represented by the grey shaded region. The GBs are separated by two (b), three (c), four (d), five (e), six (f), and seven (g) hexagons.

Supplementary Tables

Table S1: The band gap size and Schottky barrier height (SBH) of free-standing MoS_2 monolayers with GBs formed by two parallel periodic arrays of equidistant (5|7) edge dislocations, at various dislocation spacings and corresponding tilt angles. The relative reduction of band gap size and SBH is calculated with respect to the pristine free-standing MoS_2 monolayer (Eg=1.8eV[8]) and the MoS_2@Au(111) heterojunction with a physisorbed defect-free MoS_2 monolayer (SBH=1.67eV[1,9,10]), respectively.

Dislocation spacing (Å)	Tilt angle (°)	Band gap (eV)	Band gap reduction (%)	SBH (eV)	SBH reduction(%)
8.36	21.60	1.62	-10.08	0.60	-10.45
11.09	17.65	1.63	-9.61	0.61	-8.96
13.83	13.70	1.63	-9.29	0.62	-7.46

16.54	11.95	1.64	-9.11	0.63	-5.97
19.25	10.20	1.64	-9.05	0.64	-4.48

Table S2: The band gap size and SBH of free-standing MoS_2 monolayers with GBs formed by two parallel periodic arrays of equidistant (4|6) and (6|8) edge dislocations, at various dislocation spacings and corresponding tilt angles. The relative reduction of band gap size and SBH is calculated with respect to the pristine free-standing MoS_2 monolayer and the MoS_2@Au(111) heterojunction with a physisorbed defect-free MoS_2 monolayer, respectively.

Dislocation spacing (Å)	Tilt angle (°)	Band gap (eV)	Band gap reduction (%)	SBH (eV)	SBH reduction(%)
8.32	21.90	1.58	-12.08	0.56	-16.42
11.04	17.90	1.60	-11.22	0.58	-13.13
13.77	13.90	1.61	-10.54	0.60	-10.45
16.48	11.71	1.62	-10.06	0.61	-8.66
19.19	9.51	1.62	-9.80	0.62	-7.46

Table S3: The band gap size and SBH of free-standing MoS_2 monolayers with GBs formed by two parallel periodic arrays of equidistant (4|8) edge dislocations, at various dislocation spacings and corresponding tilt angles. The relative reduction of band gap size and SBH is calculated with respect to the pristine free-standing MoS_2 monolayer and the MoS_2@Au(111) heterojunction with a physisorbed defect-free MoS2 monolayer, respectively.

Dislocation spacing (Å)	Tilt angle (°)	Band gap (eV)	Band gap reduction (%)	SBH (eV)	SBH reduction(%)
8.41	48.00	1.52	-15.34	0.51	-23.73
11.29	28.00	1.55	-13.73	0.56	-16.42
14.40	21.60	1.56	-13.21	0.59	-12.24
17.50	18.00	1.57	-12.76	0.60	-10.45

Table S4: The number of Au, Mo, and S atoms, along with the total number of atoms in MoS_2 and MoS_2@Au(111) heterojunction for MoS_2 monolayer containing GBs formed by (5/7) edge dislocations. The distance between GBs is denoted by H (in hexagonal cell units), and the vertical distance between (5/7) edge dislocations along the GBs is denoted by V (in hexagonal cell units).

Sample	N(Au)	N(Mo)	N(S)	N(MoS2)	Total number of atoms
V1H6	168	38	76	114	282
V3H6	280	63	126	189	469
V5H6	364	83	166	249	613

Table S5: The number of Au, Mo, and S atoms, along with the total number of atoms in MoS_2 and MoS_2@Au(111) heterojunction for MoS2 monolayer containing GBs formed by (4/6) and (6/8) edge dislocations. The distance between GBs

is denoted by H (in hexagonal cell units), and the vertical distance between the edge dislocations along the GBs is denoted by V (in hexagonal cell units).

Sample	**Au**	**Mo**	**S**	**MoS2 atoms**	**Total number of atoms**
V1H4	120	26	52	78	198
V1H5	144	32	64	96	240
V1H6	168	38	75	113	281
V3H4	180	43	86	129	309
V3H5	240	53	106	159	399
V3H6	280	63	126	189	469
V5H4	252	55	110	165	417
V5H5	308	69	138	207	515
V5H6	364	83	166	249	613

Table S6: The number of Au, Mo, and S atoms, along with the total number of atoms in MoS_2 and MoS_2@Au(111) heterojunction for MoS_2 monolayer containing GBs formed by (4/8) edge dislocations. The distance between GBs is denoted by H (in hexagonal cell units), and the vertical distance between (4/8) edge dislocations along the GBs is denoted by V (in hexagonal cell units).

Sample	Au	Mo	S	MoS2 atoms	Total number of atoms
V1H6	192	42	84	126	318
V2H6	256	58	116	174	430
V3H6	280	66	132	198	478
V4H6	288	72	144	216	504

Citations

[1] Sorkin V, Zhou H, Yu Z G, Ang K W and Zhang Y W 2022 The effects of point defect type, location, and density on the Schottky barrier height of Au/MoS2 heterojunction: a first-principles study *Sci. Rep.* **12** 18001–15

[2] Sotthewes K, Van Bremen R, Dollekamp E, Boulogne T, Nowakowski K, Kas D, Zandvliet H J W and Bampoulis P 2019 Universal Fermi-Level Pinning in Transition-Metal Dichalcogenides *J. Phys. Chem. C* **123** 5411–20

[3] Farmanbar M and Brocks G 2016 First-principles study of van der Waals interactions and lattice mismatch at MoS2/metal interfaces *Phys. Rev. B* **93** 085304

[4] Chen W, Santos E J G, Zhu W, Kaxiras E and Zhang Z 2013 Tuning the Electronic and Chemical Properties of Monolayer MoS2 Adsorbed on Transition Metal Substrates *Nano Lett.* **13** 509–14

[5] Prada S, Martinez U and Pacchioni G 2008 Work function changes induced by deposition of ultrathin dielectric films on metals : A theoretical analysis *Phys. Rev. B* **78** 235423

[6] Kang J, Liu W, Sarkar D, Jena D and Banerjee K 2014 Computational study of metal contacts to monolayer transition-metal dichalcogenide semiconductors *Phys. Rev. X* **4** 031005

[7] Popov I, Seifert G and Tománek D 2012 Designing electrical contacts to MoS 2 Monolayers: A computational study *Phys. Rev. Lett.* **108** 156802

[8] Spirko J A, Neiman M L, Oelker A M and Klier K 2003 Electronic structure and reactivity of defect MoS2: I. Relative stabilities of clusters and edges, and electronic surface states *Surf. Sci.* **542** 192–204

[9] Sorkin V, Pan H, Shi H, Quek S Y Y and Zhang Y W 2014 Nanoscale Transition Metal Dichalcogenides: Structures, Properties, and Applications *Crit. Rev. Solid State Mater. Sci.* **39** 319–67

[10] Upadhyay S N, Satrughna J A K and Pakhira S 2021 Recent advancements of two-dimensional transition metal dichalcogenides and their applications in electrocatalysis and energy storage *Emergent Mater.* **4** 951–70